ARTICLE

Enhanced piezoelectricity of monolayer phosphorene oxides: A theoretical study

Huabing Yin,[a,b] Guangping Zheng,[b*] Jingwei Gao,[b] Yuanxu Wang,[a] and Yuchen Ma[c]

Two-dimensional (2D) piezoelectric materials have potential applications in miniaturized sensors and energy conversion devices. In this work, using first-principles simulations in different scales, we systematically study the electronic structures and piezoelectricity of a series of 2D monolayer phosphorene oxides (POs). Our calculations show that the monolayer POs have tunable band gaps along with remarkable piezoelectric properties. The calculated piezoelectric coefficient d_{11} of 54 pm/V in POs is much larger than those of 2D transition metal dichalcogenides monolayers and the widely used bulk α-quartz and AlN, and almost reaches the level of piezoelectric effect in recently discovered 2D GeS. Furthermore, two other considerable piezoelectric coefficients, i.e., d_{31} and d_{26} with −10 pm/V and 21 pm/V, respectively, are also predicted in some monolayer POs. The enhancement of piezoelectricity for monolayer phosphorene by oxidation will broaden the applications of phosphorene and phosphorene derivatives in nano-sized electronic and piezotronic devices.

1. Introduction

Piezoelectric materials, which can achieve the mechanical-electrical energy conversion, have wide application prospects in nanoscale devices, such as sensors [1, 2], actuators [3, 4], and energy harvesters [5–8]. Consequently, tremendeous efforts so far have been focused on searching for and predicting new piezoelectric materials in nanoscale and on quantifying their piezoelectricity. To realize the miniaturization of devices as well as improve their piezoelectric performances, researchers have fabricated a lot of low-dimension materials, especially two-dimensional (2D) atomically thin crystals [8–11], and found that the reduced symmetry in the layered structures of 2D materials allows them to be piezoelectric.

Theoretical calculation has become an effective tool in studying and understanding the piezoelectricity of 2D materials. For example, the calculated piezoelectric coefficient of e_{11} = 3.64×10^{-10} C/m for monolayer MoS_2 is well consistent with the experimental value of 2.9×10^{-10} C/m [11, 12]. In recent years, the piezoelectric coefficients of a lot of 2D monolayer materials, including hexagonal BN [12, 13], chemically-modified graphene [10, 14–16], metal oxides (MO, M = Be, Mg, Ca, Zn, Cd, Pb, Sr, Ba) [17, 18], metal dichalcogenides (MX_2, M = Mo, W, Cr, Nb, Ta and X = S, Se, Te) [12, 17], group IIA (or IIB) monochalcogenides (MX, M=Be, Mg, Ca, Sr, Ba, Zn, Cd and X=S, Se, Te) [17, 19], group-III monochalcogenides (MX, M = Ga, In and X = S, Se) [20, 21], group-IV monochalcogenides (MX, M = Sn, Ge and X = S, Se) [22], and group III-V semiconductors (AX, A = B, Al, Ga, In and X = N, P, As, Sb) [17, 23], have been predicted by evaluating the changes in polarization under the applied uniaxial strains. Meanwhile, it is found that the piezoelectric properties of some 2D materials mentioned above obey the periodic trends [12, 17]. More remarkably, using first-principles simulations, Fei *et al.* determined that monolayer GeS, GeSe, SnS, and SnSe are strongly piezoelectric with a huge piezoelectric coefficient of d_{11} = 75∼250 pm/V [22]. Compared to those on three-dimensional (3D) systems, investigations on 2D piezoelectricity 2D and layered materials are still in their initial research stages. Although more experiments are needed to verify the calculated results, theoretical calculations on 2D piezoelectricity could provide us with deep insights into its mechanism.

[a] *Institute for Computational Materials Science, School of Physics and Electronics, Henan University, Kaifeng 475004, China.*
[b] *Department of Mechanical Engineering, The Hong Kong Polytechnic University, Hong Kong 999077, China. E-mail: mmzheng@polyu.edu.hk*
[c] *School of Chemistry and Chemical Engineering, Shandong University, Jinan 250100, China.*

Since 2014, single-layer black phosphorene, a promising candidate for the design of electronic devices, has been introduced into 2D materials family [24, 25]. Phosphorene, which can be exfoliated from the bulk black phosphorus by using different high-yield technologies [25–27], has a puckered honeycomb structure resulted from the sp^3-hybridized P atom. Compared with other 2D materials, such as graphene and the layered transition metal dichalcogenides, phosphorene has the advantages of anisotropy, tunable direct band gaps, and unique excitonic behaviour [28–31]. Notwithstanding, a generally accepted issue of its limitation in application is the degradation because of its easy oxidation in the atmosphere [24, 25, 32, 33]. To protect the phosphorene from oxidative degradation, some air-stable materials, such as atomic-layer-deposition Al_2O_3 and few-layer hexagonal BN, are used to encapsulate the phosphorene layer away from the air [32, 34, 35]. Interestingly, Edmonds *et al.* found that phosphorene oxides (POs) formed on the few-layer black phosphorus may serve as a stable passivation layer with minimal influence on the innermost phosphorene [36]. Meanwhile, Pei *et al.* developed a new oxygen plasma etching method to fabricate air-stable phosphorene samples and precisely engineer the O-defects in the phosphorene [27]. It is shown that POs with different oxygen concentrations may result in some exciting new properties in contrast to pure phosphorene.

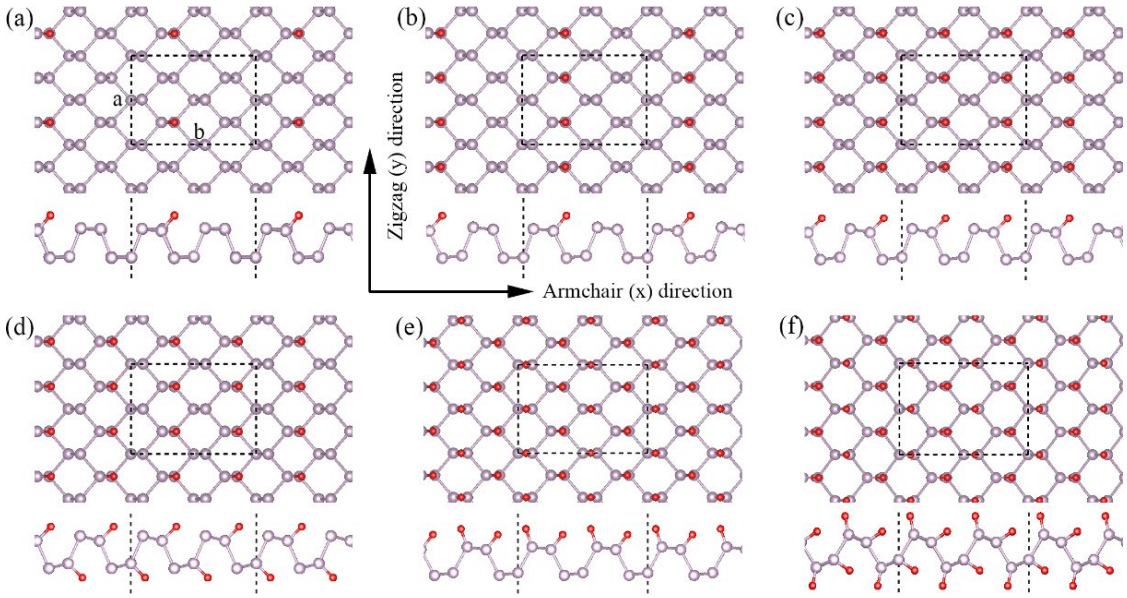

Fig. 1. Top and side views of the equilibrium structures of monolayer phosphorene oxides: (a) $P_{16}O_1$, (b) P_8O_1, (c) P_4O_1, (d) P_4O_2-I, (e) P_4O_2-II, and (f) P_4O_4. Phosphorus and oxygen atoms are represented in light purple and red, respectively. The rectangular unit cell used in the calculations is outlined by dashed line. The armchair direction and zigzag direction are defined as the *x*- and *y*-directions, respectively.

It is widely accepted that there are no piezoelectric properties in the pristine monolayer phosphorene, which has a centrosymmetric puckered structure. Nevertheless, very recently, Li *et al.* predicted a new class of 2D van der Waals crystals for phosphorus based on the ultrathin metastable phosphorus nanotube, showing that these phosphorus allotropes possess remarkable piezoelectricity with the highest coefficient of $e_{11} = -20 \times 10^{-10}$ C/m [37], which is higher than those in h-BN and MoS_2. On the other hand, similar with graphene, chemically modified phosphorene is expected to exhibit piezoelectricity. Because of its high chemical reactivity, phosphorene is easy to be oxidized at atmospheric conditions. Ziletti *et al.* have proposed the mechanisms for phosphorene oxidation and determined some stable structures of POs, such as those containing oxygen atoms in the dangling positions or in the interstitial bridges connecting phosphorus atoms [38, 39]. Wang *et al.* and Nahas *et al.* also investigated the stability, anisotropy, and electronic properties of POs, showing that the POs have the potential applications in electronic devices [40, 41]. In addition, Hao and Chen studied the mechanical properties of phosphorene nanoribbons and oxides, whereas they only paid attention to the stress-strain relations and did not provide relevant piezoelectric properties [42]. To date, there is still a lack of systematic studies on piezoelectricity in POs, which is precisely the topic we will elaborate deeply.

In this work, we investigate the electronic and piezoelectric properties of a series of monolayer POs by using first-principles density functional theory (DFT), GW method, and density functional perturbation theory (DFPT), which have achieved great success in the calculations of electronic structures and piezoelectric coefficients for other 2D materials. We will show that the monolayer POs have tunable band gaps and remarkable piezoelectric properties. Large piezoelectric coefficients predicted by our calculations will allow the monolayer POs to be used in a lot of nano-sized sensors and energy harvesting devices.

2. Models and Computational details

Fig. 1 shows all kinds of POs studied in this work. All the structures are constructed by adding 1-16 oxygen atoms on the surface of monolayer phosphorene consisting of 2×2 unit cells (16 atoms). It is noteworthy that we consider the PO with chemisorption of oxygen only at the dangling position, which has been proved to be the most stable PO adsorbed with single-oxygen atom [38]. However, when more than one oxygen atoms are adsorbed in phosphorene, PO structures with merely dangling oxygen impurities may not retain the global minimum in energy landscape, while other oxygen doping forms such as interstitial bridge impurities appear possibly in the POs [39]. Even so, the metastable states, with only dangling oxygen atoms in oxidized phosphorene, have been predicted to be stabilized kinetically in molecular dynamics simulation and synthesized possibly in experiment by Nahas *et al.* [41]. As indicated in Fig. 1(a)-(c), $P_{16}O_1$, P_8O_1 and P_4O_1 have the dangling oxygen atoms only at the top side of phosphorene. But for P_4O_2, we construct two different models, namely, P_4O_2-I and P_4O_2-II, which have double-sided and single-sided oxygen atoms, respectively. In the stoichiometric P_4O_4 configuration, each phosphorus atom adsorbs an oxygen atom on the surface, which dramatically changes the whole structural properties of the bare phosphorene, including the bond angles and bond lengths. Here, the in-plane directions x and y are defined as the armchair and zigzag directions, respectively, and z-direction is perpendicular to the monolayer.

In our studies, the geometry optimizations, elastic stiffness calculations, and piezoelectric coefficients calculations are all performed within DFT using the Vienna ab initio Simulation Package (VASP) with the projector augmented wave (PAW) approach [43–45]. For exchange and correlation energy, we use Perdew-Burke-Ernzerhof (PBE) generalized gradient approximation [46], which is the most commonly used form in the study of solids. For DFT calculations, a cut-off energy of 750 eV for the plane wave basis set and a 10×14×1 Monkhorst-Pack k-points have been used. The convergence criteria for electronic and ionic relations are 10^{-6} eV and 10^{-3} eV/Å, respectively. A 20 Å vacuum space is added in the z-direction to prevent the periodic interactions among atoms.

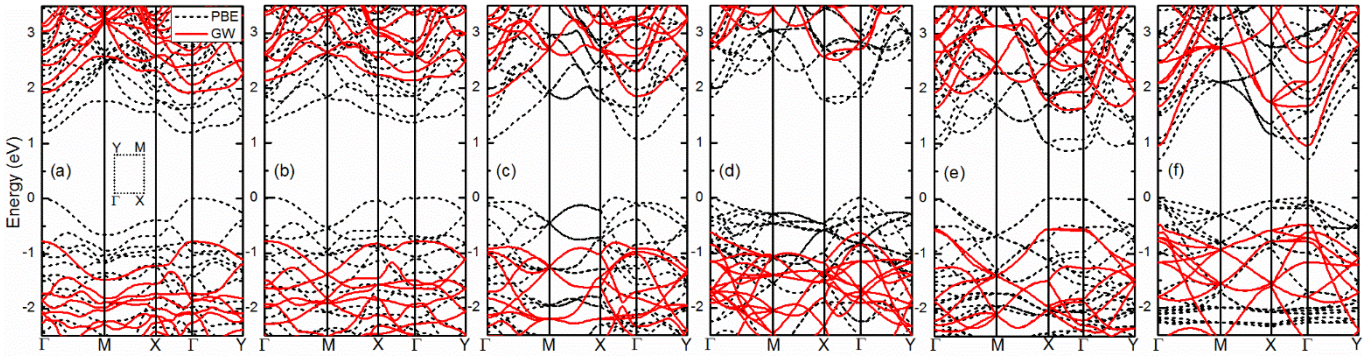

Fig. 2. Calculated band structures of monolayer phosphorene oxides using DFT-PBE (black dotted line) and *GW* (red solid line) methods: (a) $P_{16}O_1$, (b) P_8O_1, (c) P_4O_1, (d) P_4O_2-I, (e) P_4O_2-II, and (f) P_4O_4. The valence band maximum (VBM) in the DFT-PBE calculation is taken as zero of the energy scale.

It is generally known that ground-state DFT-PBE usually fails to correctly predict the band gaps of solids [47], especially when using standard local or semi-local approximations to the exchange-correlation potentials. Thus, we examine the electronic band structures of phosphorene oxides using *GW* method [48], which is performed by a set of Gaussian-orbital based codes [49–51]. In *GW* procedure, DFT-PBE calculations are carried out firstly to get the Kohn-Sham eigenvalues and eigenfunctions that will be used to construct self-energy operators. Then, the *GW* calculations are usually performed within first-order perturbation theory by assuming that the quasiparticle wave functions can be approximated by DFT Kohn-Sham eigenfunctions. As mentioned in our previous works [52, 53], the basis set for all steps of *GW* calculations is made by atom-centered Gaussian orbitals.

The relaxed-ion elastic stiffness coefficients, C_{ijkl}, including both the ionic and electronic contributions [54], are calculated by using finite difference method as implemented in VASP code. Meanwhile, DFPT method and Berry's Phase approximation [54–56], which have been proved to be two of the most effective methods in evaluating the piezoelectricity of 2D materials [12, 17–19, 22], are applied to calculate relaxed-ion piezoelectric coefficients, e_{ijk}, including both the ionic and electronic contributions. We perform the DFPT and polarization vector calculations by using the LEPSILON tag and LCALCPOL tag in VASP code, respectively. Essentially, according to the definitions, the elastic stiffness and piezoelectric coefficients, C_{ijkl}, e_{ijk}, and d_{ijk}, can be evaluated by

$$C_{ijkl} = \frac{d\sigma_{ij}}{d\varepsilon_{kl}}, \quad (1)$$

$$e_{ijk} = \frac{dP_i}{d\varepsilon_{jk}}, \quad (2)$$

$$e_{ijk} = \frac{dP_i}{d\sigma_{jk}}, \quad (3)$$

where σ_{ij}, ε_{kl}, and P_i represent the stress tensor, strain tensor, and polarization tensor, respectively [57]. The subscripts i=1, 2, and 3 for polarization tensor P_i indicate the polarization components along *x*-, *y*-, and *z*-directions, respectively. In Voigt

notation [57], the subscripts *i and j* for the components of σ_{ij}, ε_{ij} can be indicated as 1 = *xx*, 2= *yy*, 3 = *zz*, 4 = *yz*, 5 = *zx*, and 6 = *xy*. For 2D systems, only 1 (*xx*), 2 (*yy*), and 6 (*xy*) components for stress and strain tensors need to be considered in the calculations. Hence, the 2D elastic and piezoelectric tensors in Eqs. (1)−(3) can be also written as

$$C_{ij} = \begin{pmatrix} C_{11} & C_{12} & C_{16} \\ C_{21} & C_{22} & C_{26} \\ C_{61} & C_{62} & C_{66} \end{pmatrix}, \quad (4)$$

$$e_{ij} = \begin{pmatrix} e_{11} & e_{12} & e_{16} \\ e_{21} & e_{22} & e_{26} \\ e_{31} & e_{32} & e_{36} \end{pmatrix}, \quad (5)$$

$$d_{ij} = \begin{pmatrix} d_{11} & d_{12} & d_{16} \\ d_{21} & d_{22} & d_{26} \\ d_{31} & d_{32} & d_{36} \end{pmatrix}, \quad (6)$$

where $e_{ik} = d_{ij}C_{jk}$ [57]. Particularly, in Eqs. (4), some quantities are equal, such as $C_{12} = C_{21}$, $C_{16} = C_{61}$, and $C_{26} = C_{62}$. The high symmetry of 2D systems can effectively reduce the number of independent elastic stiffness and piezoelectric coefficients. Because the original symmetry of phosphorene is destroyed by adding the dangling oxygen atoms on the surface, for the structures investigated, all the piezoelectric coefficients in Eqs. (5)−(6) will be calculated. As mentioned above, here we only consider the relaxed-ion elastic stiffness and piezoelectric coefficients which include both the ionic and electronic contributions.

TABLE 1. DFT calculated structural parameters (in Å) and band gaps (in eV) calculated by DFT and *GW* methods for monolayer 2×2 phosphorene and phosphorene oxides. The direct band gap is defined as the energy gap at Γ point.

			Band gap/PBE		Band gap/*GW*	
materia	a	b	Indirect	direct	Indirect	direct
2×2 P	9.26	6.60		0.93		2.32
$P_{16}O_1$	9.28	6.61		1.18		2.68
P_8O_1	9.28	6.64		1.38		2.92
P_4O_1	9.37	6.68	1.07	1.16	2.67	2.78
P_4O_2-I	9.46	6.79	1.73	1.84	3.14	3.34
P_4O_2-II	10.14	6.91	0.87	0.92	2.16	2.21
P_4O_4	10.24	7.28		0.70		1.44

TABLE 2. Calculated non-zero elastic stiffness coefficients C_{ij} of monolayer phosphorene and phosphorene oxides. C_{ij} is in units of N/m.

material	C_{11}	C_{22}	C_{66}	C_{12}
2×2 P	23.7	103.2	22.4	16.9
$P_{16}O_1$	25.6	99.2	23.0	15.5
P_8O_1	25.8	96.1	23.6	14.5
P_4O_1	36.8	92.0	25.6	15.4
P_4O_2-I	40.4	85.2	30.1	14.3
P_4O_2-II	15.0	67.4	21.3	0.45
P_4O_4	25.1	50.3	17.2	6.6

3. Results and discussion

The DFT-optimized structural parameters (*a* and *b*) and *GW* and DFT-PBE predicted band gaps of monolayer phosphorene and POs are summarized in Table 1. The results vary apparently with different PO models. We found the lattice constants of pristine phosphorene to be *a* = 4.63 Å and *b* = 3.30 Å, in agreement with other calculated results [39, 58]. In comparison with those of phosphorene oxides, in Table 1, results are listed for monolayer phosphorene with a 2×2 unit cell. With increasing concentration of dangling oxygen atoms in the POs, which is changed from 1/17 of $P_{16}O_1$ to 1/2 of P_4O_4, the lattice constants of a and *b* increase by roughly 1.0 Å and 0.7 Å, respectively. In the meantime, the inclusion of dangling oxygen on the surface and formation of POs may effectively modify the electronic properties of phosphorene. It is known that monolayer phosphorene has a direct gap at Γ point. In our DFT-PBE calculation, the band gap of monolayer phosphorene is about 0.93 eV, and within *GW* calculation the band gap is enlarged to 2.32 eV, which is consistent with those obtained from previous *GW* studies and experimental results [58, 59]. As shown in Table 1 and Fig. 2, chemisorption of oxygen atoms drastically changes the band structure of phosphorene. The nature of band gap depends on the relative proportion of oxygen atoms in the POs and an indirect band gap is predicted for P_4O_1, P_4O_2-I, and P_4O_2-II. To facilitate our comparison, we define the direct band gap as the energy gap at Γ point. Besides, by using *GW*, a direct band gap is obtained for other POs monolayers, i.e., $P_{16}O_1$, P_8O_1, and P_4O_4. Furthermore, the calculated *GW* band gaps for P_4O_2-II and P_4O_4 are indirect and direct with values of 2.16 eV and 1.44 eV, respectively, which are all smaller than that calculated for pristine phosphorene (2.32 eV at *GW* level obtained in this work). The nature of small band gaps for some POs may lead to new properties, for example, high carrier mobility and low-energy optical absorption and photoluminescence [27, 29]. Studies on the optical properties of narrow band-gap POs are underway.

To determine the piezoelectric coefficients based on Eqs. (4)-(6), we first calculate the elastic stiffness coefficients C_{ij} in Eqs. (4) for the POs by using finite difference method, which can be directly performed in VASP code. As mentioned in the calculation methods, the elastic stiffness coefficients are C_{ji} with *i* and *j* being equal to 1, 2, or 6, and the values of C_{26} and C_{16} coefficients are found to be zero in the bare phosphorene and POs. Hence only the independent non-zero coefficients C_{11}, C_{22}, C_{66}, and C_{12} are given in Table 2. Meanwhile, the elastic stiffness coefficients of pristine phosphorene are also calculated. In order to compare the Young's moduli of monolayer phosphorene with those calculated in previous studies, we choose the interlayer spacing *d* = 5.29 Å of bulk black phosphorus to be the effective thickness of monolayer phosphorene. Then we transform the units of elastic stiffness coefficients and Young's muduli in 2D (N/m) into those in 3D

(N/m^2 or GPa). The 2D effective Young's moduli along the *x*- and *y*-directions, E_x and E_y respectively, can be derived as

$$E_x = \frac{C_{11}C_{22} - C_{12}^2}{C_{22}}, \quad E_y = \frac{C_{11}C_{22} - C_{12}^2}{C_{11}}, \qquad (7)$$

while the 3D Young's muduli Y_x and Y_y of monolayer phosphorene can be determined as

$$Y_x = \frac{E_x}{d}, \quad Y_y = \frac{E_y}{d}, \qquad (8)$$

where *d* is the effective thickness. Combining Eqs. (7) and Eqs. (8) and using C_{ij} listed in Table 2, the 3D (2D) Young's muduli Y_x (E_x) and Y_y (E_y) of monolayer phosphorene are calculated to be 40 GPa (20.9 N/m) and 172 GPa (91.1 N/m), respectively, which are in agreement with previous calculated results [60]. The results demonstrate that the elastic stiffness coefficients calculated in this work by the finite difference method are absolutely reliable.

With the increase in oxygen concentration, the elastic stiffness coefficients of POs definitely go through some changes. For example, as listed in Table 2, C_{22} coefficient decreases by about 50% when the system is changed from $P_{16}O_1$ to P_4O_4. Although the C_{11} and C_{66} coefficients do not change that much, the P_4O_2-I structure possesses the largest C_{11} and C_{66} of 40.4 N/m and 30.1 N/m, respectively. Furthermore, it is found that P_4O_2-II has the smallest C_{11} and C_{12} coefficients (15 N/m and 0.45 N/m, respectively), which differ with those of other POs. The unusual mechanical properties of P_4O_2-II may lead to the enhanced piezoelectricity, which will be discussed in the sections that follow.

In this work, the piezoelectric properties of POs were calculated by using both DFPT method and DFT-based Berry's phase technique. The DFPT method in VASP, which can directly provide all the piezoelectric tensors for the electronic and ionic contributions [18], is much simpler than the Berry's phase approximation. We have summarized in Table 3 the piezoelectric coefficients e_{ij}, e.g., e_{11}, e_{12}, e_{26}, e_{31}, and e_{32}, calculated by DFPT method. It should be noted that other four coefficients e_{13}, e_{21}, e_{22}, and e_{36} in Eqs. (5) are nearly zero for all POs models and are not listed. From the perspective of mechanical-electrical energy conversion, the d_{ij} coefficients, which can be obtained through matrix operations with e_{ij} and C_{ij} coefficients, are the most useful piezoelectric coefficients and decide the conversion efficiency. Thus, the corresponding d_{ij} coefficients for the POs are also calculated and summarized in Table 3.

Based on Eqs. (2) and the Berry's phase technique [55, 56], the piezoelectric tensors e_{ij} can be obtained by a linear fitting of the polarization change per area *vs*. the strain ε applied to the orthorhombic unit cell. Taking the dominant e_{11} coefficient of POs monolayers as an example, we first apply the uniaxial stain ε_{11} which is changed from −0.01 to 0.01 with a step of 0.005, to the unit cell along *x*-direction, and then the 2D polarization change ΔP_1 along *x*-direction is calculated in DFT method and evaluated by the modern theory of polarization. It is noted that in this process the atomic positions for every strain state are fully relaxed in order to calculate the relax-ion coefficients. Finally, a linear fitting of ΔP_1 with respect to ε_{11} is performed to obtain the piezoelectric coefficient e_{11}, derived from the slope of the line. In Fig. 3(a), the linear relationships between the polarization change and uniaxial strain for the six POs monolayers are illustrated. As shown in Fig. 3(b), the difference in e_{11} coefficients calculated by DFPT method and obtained by DFT-based Berry's phase method is rather small. Obviously, for all POs monolayers, Berry's phase method can give slightly larger e_{11} coefficients than the DFPT method.

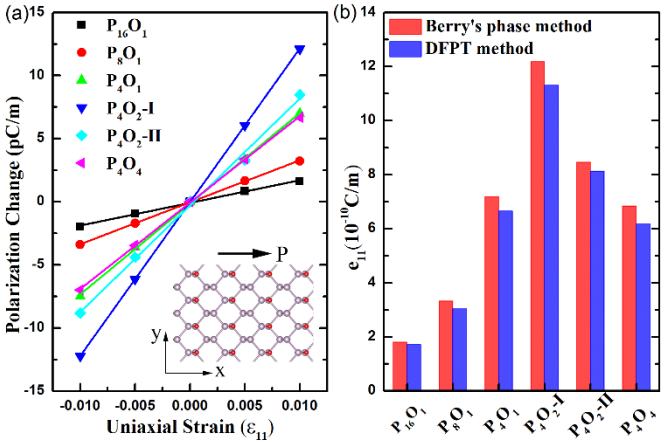

Fig. 3. (a) Calculated unit-cell polarization change per area along *x*-direction under the applied uniaxial strain (ε_{11}) along x-direction for the monolayer POs. (b) Comparison of the piezoelectric coefficients e_{11} of the monolayer POs calculated by the DFPT method and Berry's phase method, respectively. The piezoelectric coefficients e_{11} based on Berry's phase technique can be obtained from the slope of lines through linear fitting of the polarization change vs. ε_{11} in (a).

In Table 3, we can see that the concentration and position of dangling oxygen atoms can effectively influence the piezoelectricity of monolayer POs varying from $P_{16}O_1$ to P_4O_2. For instance, the main piezoelectric coefficient d_{11} increases with increasing oxygen concentration, and the P_4O_2-II monolayer possesses the largest piezoelectric effect (d_{11} = 54.02 pm/V, d_{12} = 4.97 pm/V, and d_{31} = −10.01 pm/V). The oxygen-concentration dependent piezoelectric coefficients could be related to the enhancement of the polarizability with the inclusion of oxygen atoms. The calculated d_{11} coefficients for monolayer POs (6.56−54.06 pm/V) are generally larger than those for some conventional 2D piezoelectric materials, such as MoS_2, BN, and GaSe (d_{11} = 3.73 pm/V [12], d_{11} = 0.60 pm/V [12], and d_{11} = 2.30 pm/V [20], respectively), but smaller than those for the recently emerging monolayer group-IV monochalcogenides, including SnSe, SnS, GeSe, and GeS, which have been predicted to possess huge d_{11} coefficients (about 75−250 pm/V) [22]. Compared to the d_{11} coefficients, the values of d_{12} coefficients for monolayer POs are much smaller, except for that (d_{12} = 4.97 pm/V) for P_4O_2-II monolayer.

Due to the chemisorption of oxygen atoms on the surface of monolayer phosphorene, the polarizability of POs along the *z*-

direction and perpendicular to the monolayer produces certain changes, such as the increase of out-of-plane piezoelectric coefficients d_{31} and d_{32} with increasing concentration of single-sided oxygen, as listed in Table 3. In particular, P_4O_2-II has the largest d_{31} and d_{32} coefficients of −10.01 pm/V and −1.92 pm/V, respectively, which are much larger than those of graphene oxide (d_{31} = 0.24 pm/V) [15] and 2D buckled hexagonal AlAs compound (d_{31} = 0.57 pm/V) [17]. However, for P_4O_2-I and P_4O_4 monolayers with double-sided oxygen atoms, the polarizability along z-direction can balance with each other, resulting in the d_{31} and d_{32} coefficients which are practically zero. Interestingly, a new piezoelectric effect in 2D materials is reported in this study, which has not been well explored in previous researches. As listed in Table 3, the d_{26} coefficient is much high for monolayer POs, which represents the piezoelectric effect of significant polarization change along *y*-direction with the applied shear strain on the *xy*-plane. It can be found that the d_{26} coefficients for P_4O_2-I and P_4O_4 monolayers exhibit the largest values of 21.26 pm/V and 21.40 pm/V, respectively, suggesting the great influences of shear strains on the in-plane polarization in the monolayer POs.

TABLE 3. Calculated piezoelectric coefficients e_{ij} and d_{ij} of monolayer POs by using DFPT method. e_{ij} and d_{ij} are in units of 10^{-10} C/m and pm/V, respectively.

material	e_{11}	e_{12}	e_{26}	e_{31}	e_{32}	d_{11}	d_{12}	d_{26}	d_{31}	d_{32}
$P_{16}O_1$	1.72	1.28	0.73	-0.22	-0.20	6.56	0.27	3.17	-0.81	-0.07
P_8O_1	3.04	2.28	1.60	-0.40	-0.33	11.42	0.65	6.78	-1.48	-0.12
P_4O_1	6.65	3.17	0.00	-0.92	-0.62	17.88	0.45	0.00	-2.39	-0.27
P_4O_2-I	11.31	3.83	6.40	0.00	0.00	28.07	-0.22	21.26	0.00	0.00
P_4O_2-II	8.13	3.59	1.58	-1.51	-1.34	54.06	4.97	7.42	-10.01	-1.92
P_4O_4	6.18	0.90	3.68	0.00	0.00	25.01	1.49	21.40	0.00	0.00

In recent studies, Li *et al.* have predicted a new class of 2D phosphorus allotropes with remarkable high stabilities and piezoelectricity to tackle the problems of non-piezoelectric properties of black phosphorene and blue phosphorene [37]. In this work, from another perspective, we demonstrate that the piezoelectricity could be enhanced in monolayer black phosphorene by the oxidation and consequently the formation of monolayer POs. The band gaps and piezoelectric coefficients of the POs can be tuned by the concentration and position of chemisorption oxygen atoms in these 2D materials. As mentioned above, we only consider the chemisorption of dangling oxygen atoms on the surface of monolayer phosphorene, i.e., P=O bonding, and some POs with high oxygen concentrations may be in metastable states [39, 41, 61]. For example, very recently, Luo and Xiong have predicted some low-energy structures of 2D monolayer POs based on a global optimization approach and determined that P−O−P motifs will exist when the oxygen concentration is high [61]. However, the excellent piezoelectricity of the POs explored in this study could reflect the physical properties of those layered POs compounds with similar chemical compositions and thus is of general significance for 2D materials. Other most stable monolayer POs may be also strongly piezoelectric. More importantly, in experiments, Pei *et al.* have reported that the oxygen defects in the phosphorene monolayer could be precisely engineered by using O_2 plasma etching technique [27]. Thus, it is expected that an increasing number of 2D monolayer POs materials with higher stability and piezoelectricity will be synthesized and the theoretical results reported in this work would be compared with those in experiments.

4. Conclusions

In summary, we have investigated the electronic and piezoelectric properties of 2D monolayer POs structures using first-principles methods, i.e., DFT, *GW*, and DFPT. Our calculations clearly show that these monolayer POs are excellent piezoelectric materials. The band gaps of POs, ranging from the direct band gap of 1.44 eV for P_4O_4 to the indirect band gap of 3.14 eV for P_4O_2-I, can be tuned by the chemisorption of oxygen atoms with different concentrations and positions. The smaller direct band gap of monolayer POs compared with that of phosphorene may induce some exciting optical properties. The monolayer POs materials have large in-plane and out-of-plane piezoelectric coefficients, i.e., d_{11} of 54 pm/V and d_{31} of −10 pm/V for P_4O_2-II structure and d_{26} of 21 pm/V for P_4O_2-I and P_4O_4 structures, demonstrating huge piezoelectric effects in these 2D materials. The remarkable piezoelectricity allows the monolayer POs materials to have potential applications in electronic and piezotronic devices, such as sensors, actuators, and energy harvesters. In spite of the high chemical reactivity of black phosphorene monolayer, through modern experimental techniques, various POs monolayers are highly possible to be engineered and synthesized in the near future. Meanwhile, we believe that the chemisorption of other types of atoms, e.g., fluorine or hydrogen, might also enhance the piezoelectric effects in the phosphorene monolayer. The theoretical calculations reported here show that the chemical modification is effective in improving the piezoelectric properties of 2D non-piezoelectric materials, which has been successfully applied to graphene materials.

Acknowledgements

This work was supported by the National Natural Science Foundation of China (Grants Nos. 21603056), the Hong Kong Scholars Program (XJ2016045), and a grant from the Research Grants Council of the Hong Kong Special Administrative Region, China (GRF15260716).

References

1 C. Stampfer, T. Helbling, D. Obergfell, B. Scho¨berle, M. K. Tripp, A. Jungen, S. Roth, V. M. Bright, and C. Hierold, Nano Lett. 6, 233 (2006).
2 A. I. Kingon1 and S. Srinivasan, Nat. Mater. 4, 233 (2005).
3 A. M. Fennimore, T. D. Yuzvinsky, W.-Q. Han, M. S. Fuhrer, J. Cumings, and A. Zettl, Nature 424, 408 (2003).
4 S. Park, J. An, J. W. Suk, and R. S. Ruoff, Small 6, 210 (2010).
5 Z. L. Wang and J. Song, Science 312, 242 (2006).
6 R. Yang, Y. Qin, L. Dai, and Z. L. Wang, Nat. Nanotechnol. 4, 34 (2009).
7 E. Lee, J. Park, M. Yim, Y. Kim, and G. Yoon, Appl. Phys. Lett. 106, 023901 (2015).
8 W. Wu, L. Wang, Y. Li, F. Zhang, L. Lin, S. Niu, D. Chenet, X. Zhang, Y. Hao, T. F. Heinz, et al., Nature 514, 470 (2014).
9 I. Naumov, A. M. Bratkovsky, and V. Ranjan, Phys. Rev. Lett. 102, 217601 (2009).
10 M. T. Ong and E. J. Reed, ACS Nano 6, 1387 (2012).
11 H. Zhu, Y. Wang, J. Xiao, M. Liu, S. Xiong, Z. J. Wong, Z. Ye, Y. Ye, X. Yin, and X. Zhang, Nat. Nanotechnol. 10, 151 (2015).
12 K.-A. N. Duerloo, M. T. Ong, and E. J. Reed, J. Phys. Chem. Lett. 3, 2871 (2012).
13 K. H. Michel and B. Verberck, Phys. Rev. B 80, 224301 (2009).
14 M. T. Ong, K.-A. N. Duerloo, and E. J. Reed, J. Phys. Chem. C 117, 3615 (2013).
15 Z. Chang, W. Yan, J. Shang, and J. Z. Liu, Appl. Phys. Lett. 105, 023103 (2014).
16 M. Noor-A-Alam and Y.-H. Shin, Phys. Chem. Chem. Phys. 18, 20443 (2016).
17 M. N. Blonsky, H. L. Zhuang, A. K. Singh, and R. G. Hennig, ACS Nano 9, 9885 (2015).
18 M. M. Alyoruk, Phys. Status Solidi B 253, 2534 (2016).
19 C. Sevik, D. Cakır, O. Gulseren, and F. M. Peeters, J. Phys. Chem. C 120, 13948 (2016).
20 W. Li and J. Li, Nano Res. 8, 3796 (2015).
21 Y. Guo, S. Zhou, Y. Bai, and J. Zhao, Appl. Phys. Lett. 110, 163102 (2017).
22 R. Fei, W. Li, J. Li, and L. Yang, Appl. Phys. Lett. 107, 173104 (2015).
23 R. Gao and Y. Gao, Phys. Status Solidi RRL 11, 1600412 (2017).
24 L. Li, Y. Yu, G. J. Ye, Q. Ge, X. Ou, H. Wu, D. Feng, X. H. Chen, and Y. Zhang, Nat. Nanotechnol. 9, 372 (2014).
25 H. Liu, A. T. Neal, Z. Zhu, Z. Luo, X. Xu, D. Toma´nek, and P. D. Ye, ACS Nano 8, 4033 (2014).
26 P. Yasaei, B. Kumar, T. Foroozan, C. Wang, M. Asadi, D. Tuschel, J. E. Indacochea, R. F. Klie, and A. SalehiKhojin, Adv. Mater. 27, 2887 (2015).
27 J. Pei, X. Gai, J. Yang, X. Wang, Z. Yu, D.-Y. Choi, B. Luther-Davies, and Y. Lu, Nat. Commun. 7, 10450 (2016).
28 V.Tran, R. Soklaski, Y. Liang, and L. Yang, Phys. Rev. Lett. 89, 235319 (2014).
29 R. Xu, J. Yang, Y. W. Myint, J. Pei, H. Yan, F. Wang, and Y. Lu, Adv. Mater. 28, 3493 (2016).
30 A. Castellanos-Gomez, J. Phys. Chem. Lett. 6, 4280 (2015).
31 X. Ling, H. Wang, S. Huang, F. Xia, and M. S. Dresselhaus, Proc. Natl. Acad. Sci. U.S.A. 112, 4523 (2015).
32 J. D. Wood, S. A. Wells, D. Jariwala, K.-S. Chen, E. Cho, V. K. Sangwan, X. Liu, L. J. Lauhon, T. J. Marks, and M. C. Hersam, Nano Lett. 14, 6964 (2014).
33 S. P. Koenig, R. A. Doganov, H. Schmidt, A. H. C. Neto, and B. Ozyilmaz, Appl. Phys. Lett. 104, 103106 (2014).
34 J. Na, Y. T. Lee, J. A. Lim, D. K. Hwang, G.-T. Kim, W. K. Choi, and Y.-W. Song, ACS Nano 8, 11753 (2014).
35 A. Avsar, I. J. Vera-Marun, J. Y. Tan, K. Watanabe, T. Taniguchi, A. H. C. Neto, and B. ¨Ozyilmaz, ACS Nano 9, 4138 (2015).
36 M. T. Edmonds, A. Tadich, A. Carvalho, A. Ziletti, K. M. O'Donnell, S. P. Koenig, D. F. Coker, B. Ozyilmaz, A. H. C. Neto, and M. S. Fuhrer, ACS Appl. Mater. Interfaces 7, 14557 (2015).
37 Z. Li, C. He, T. Ouyang, C. Zhang, C. Tang, R. A. Romer, and J. Zhong, arXiv:1701.05075 (2017).
38 A. Ziletti, A. Carvalho, D. K. Campbell, D. F. Coker, and A. H. C. Neto, Phys. Rev. Lett. 114, 046801 (2015).
39 A. Ziletti, A. Carvalho, P. E. Trevisanutto, D. K. Campbell, D. F. Coker, and A. H. C. Neto, Phys. Rev. B 91, 085407 (2015).
40 G. Wang, R. Pandey, and S. P. Karna, Nanoscale 7, 524 (2015).
41 S. Nahas, B. Ghosh, S. Bhowmick, and A. Agarwal, Phys. Rev. B 93, 165413 (2016).
42 F. Hao and X. Chen, J. Appl. Phys. 118, 234304 (2015).
43 G. Kresse and J. Furthmulle, Comput. Mat. Sci. 6, 15 (1996).
44 G. Kresse and J. Furthmulle, Phys. Rev. B 54, 11169 (1996).
45 G. Kresse and D. Joubert, Phys. Rev. B 59, 1758 (1999).
46 J. P. Perdew, K. Burke, and M. Ernzerhof, Phys. Rev. Lett. 77, 3865 (1996).
47 M. S. Hybertsen and S. G. Louie, Phys. Rev. Lett. 55, 1418 (1985).
48 G. Onida, L. Reining, and A. Rubio, Rev. Mod. Phys. 74, 601 (2002).
49 M. Rohlfing, P. Kruger, and J. Pollmann, Phys. Rev. B 48, 17791 (1993).
50 M. Rohlfing, P. Kruger, and J. Pollmann, Phys. Rev. B 52, 1905 (1995).
51 M. Rohlfing and S. G. Louie, Phys. Rev. B 62, 4927 (2000).
52 J. Mu, Y. Ma, H. Yin, C. Liu, and M. Rohlfing, Phys. Rev. Lett. 111, 137401 (2013).
53 H. Yin, Y. Ma, J. Mu, C. Liu, and M. Rohlfing, Phys. Rev. Lett. 112, 228301 (2014).
54 X. Wu, D. Vanderbilt, and D. R. Hamann, Phys. Rev. B 72, 035105 (2005).
55 R. D. King-Smith and D. Vanderbilt, Phys. Rev. B 47, 1651 (1993).
56 D. Vanderbilt, J. Phys. Chem. Solids 61, 147 (2000).
57 J. F. Nye, Physical Properties of Crystals: Their Representation by Tensors and Matrices (Oxford University Press, USA, 1985).
58 D. Cakır, C. Sevik, and F. M. Peeters, Phys. Rev. B 92, 165406 (2015).
59 X. Wang, A. M. Jones, K. L. Seyler, V. Tran, Y. Jia, H. Zhao, H. Wang, L. Yang, X. Xu, and F. Xia, Nat. Nanotechnol. 10, 517 (2015).
60 Q. Wei and X. Peng, Appl. Phys. Lett. 104, 251915 (2014).
61 W. Luo and H. Xiang, Angew. Chem. Int. Ed. 55, 8575 (2016).